Southern Ocean Origin of Multidecadal Variability in the North Brazil Current

RENÉ M. VAN WESTEN, FIONA R. VAN DER BURGT, HENK A. DIJKSTRA AND WILL P.M. DE RUIJTER

Institute for Marine and Atmospheric Research Utrecht, Utrecht University, Utrecht, the Netherlands

ABSTRACT

A new mode of multidecadal variability in the Southern Ocean, the so-called Southern Ocean Mode (SOM), has recently been discovered by Le Bars et al. (2016) in the strongly eddying version of the Parallel Ocean Program (POP). This mode has a corresponding period of 40 – 50 years and affects the variability in the Atlantic Meridional Overturning Circulation (AMOC) and the North Brazil Current (NBC). Using multichannel singular spectral analysis on the POP output, also multidecadal variability was found in the NBC. This result suggests a teleconnection between the Southern Ocean and the NBC. The northward propagating multidecadal signal is clearly visible in SSH in the Southern Ocean, but submerges at 40°S. Anomalies in ocean heat content and temperature are observed between 40° – 5°S, at depths up to 1 km, and re-emerge near the equator where the anomalies propagate towards the NBC. This provides the evidence that the multidecadal signal found in the NBC has a Southern Ocean origin, and hence connected to the SOM.

1. Introduction

The Southern Ocean Mode (SOM) has recently been discovered in a state-of-the-art eddy resolving ocean model by Le Bars et al. (2016). This mode has a multidecadal variability of 40 – 50 years and has a significant influence on the ocean heat content (OHC). The interaction between the general circulation and eddies cause the appearance of the SOM. The SOM is absent in a non eddy resolving model, underlining the importance of eddies in the SOM mechanism and on the general circulation (Hallberg 2013; Le Bars et al. 2016). Using modeled data has an advantage over historic records in studing the multidecadal variability in OHC, since the model output provides longer time series. Besides, historic records and observations of the OHC show discrepancies due to the changes in observation networks (Cheng and Zhu 2014). Studying directly the multidecadal variability in OHC from observations is therefore an enormous task. The usage of an high resolution model (as in Le Bars et al. (2016)) can overcome this problem and providing longer time series.

The SOM influences the multidecadal variability in the Atlantic Meridional Overturning Circulation (AMOC) (Le Bars et al. 2016), leading to a teleconnection with the northern hemispheric part of the Atlantic Ocean. However, this teleconnection has not been investigated yet. The North Brazil Current (NBC) is located in the Atlantic Ocean and is directly influenced by the AMOC (Rühs et al. 2015). Therefore, there might be a signal of multidecadal variability in the NBC originating from the Southern Ocean. This teleconnection might give some insights on how the OHC anomalies are distributed and shed some light on changes in OHC from observations (Cheng and Zhu 2014).

The NBC current is highly variable in time and a retroflection is present near 8°N (Csanady 1985; Fratantoni and Glickson 2002; Condie 1991). Even if the multidecadal variability is detected in the NBC, it is possible that on short time scales ($<$ 3 months) the model fails to resolve the NBC correctly. This will question the robustness of the multidecadal variability in the NBC. Therefore, it is necessary to validate the intrinsic behavior of the NBC with altimetry data before investigating the multidecadal variability. This provides a reference of the capability of the model and supports the results of the multidecadal variability in this region.

In this study we want to investigate whether there is a multidecadal signal near the NBC and whether a teleconnection is present with the Southern Ocean (Le Bars et al. 2016). Since the multidecadal variability is only present in an eddy resolving ocean model, the model needs to be validated with altimetry data for short time scales ($<$ 3 months) before analyzing the multidecadal variability near the NBC. We use different analysis tools to detect significant oscillations within the field of interest. These tools will be introduced in the corresponding subsections. The results of our findings are presented in the results section, followed by a discussion.

2. Data Access and Models

The modeled data provided by the Parallel Ocean Program (POP) (Smith et al. 2010) has a high resolution of 0.1°, transformed back onto a rectangular grid with grid sizes of $0.4^\circ \times 0.4^\circ$. This model is capable of resolving the internal Rossby deformation radius (Hallberg 2013) and is strongly eddying. The data of POP is generated while using a constant CO_2-level, a so-called control run. This control run has a spin-up of 75 years to adjust the model to an equilibrium. The POP output are mainly available for monthly averages, but daily averages are also available (Le Bars et al. 2016). Weekly averages will be generated from daily averages.

The monthly data sets contain the three dimensional velocity field, kinetic energy, temperature, salinity, SSH, wind-stress and depth of the mixed layer over more than 200 years (2415 months). In addition, these monthly quantities are resolved at 42 depth levels reaching depths up to 5500 m. The wind forcing was determined from a climatology mean and using a standard bulk formulae (Le Bars et al. 2016). The wind forcing is constant near the NBC. The daily data sets only resolve the velocity field, temperature and salinity near the surface (5 and 15 m depth) and SSH over a period of four years (208 weeks).

To test whether the multidecadal variability is also present in observations, we used the reanalyzed data set of the Simple Ocean Data Assimilation (SODA[1]) version 2.2.4. The data set has a grid resolution of $0.5^\circ \times 0.5^\circ$ and a time span from 1871 – 2010, containing 1680 monthly fields. The data set is capable of resolving the horizontal and vertical velocity field, temperature, salinity, SSH and wind-stress. These monthly quantities are resolved at 40 depth levels, similar to POP. The data assimilation has different input from ship intake to remotely sensed sea surface temperature. Full details of this data set are described by Carton and Giese (2008). This data set is not an eddy resolving ocean model.

We obtained the altimetry data from the Archiving, Validation and Interpretation of Satellite Oceanographic data base (AVISO[2]) during the period of 1993 – 2013. The data are composed of daily averages of gridded geostrophic velocity and SSH and is available on a rectangular grid with grid sizes of $0.25^\circ \times 0.25^\circ$. The actual time resolution is approximately ten days and spatial resolution of 1° (Le Bars et al. 2014). Weekly and monthly averages are generated using the daily data, producing 1095 weekly and 252 monthly averages of geostrophic velocity and SSH.

First the capability of POP is tested against AVISO for short time scales, based on position and seasonality of the NBC retroflection. It is possible to deduce whether rings are shed off and spatial-temporal variations are present in the field of interest. We used 208 weekly and 600 monthly averages for POP from model year 266 – 269 and 205 – 254, respectively. The multidecadal variability are analyzed over all available months of POP and SODA, while using quantities such as SSH, temperature, salinity and velocity.

3. Data Analysis Methods

a. Multi-channel Singular Spectrum Analysis

The multichannel singular spectrum analysis (M-SSA) (Ghil et al. 2002) is an analysis tool which can be used to study spatial-temporal variations. This analysis tool reveals dominant oscillations within a given field (i.e. SSH in the NBC). Each individual time series will be lagged by a total lag of M, creating M lagged copies of each individual time series, and studying the interrelationship of all these lagged time series (Plaut and Vautard 1994). In addition, it is possible to apply a Monte Carlo significance test to determine whether oscillations can be distinguished from red noise with a certain confidence interval (Allen and Robertson 1996; Allen and Smith 1996). After performing the M-SSA, it is possible to find pairs of space-time principal components (ST-PCs) (Schmeits and Dijkstra 2000). These ST-PCs pairs can be used to determine the reconstructed components (RCs) which reveal solely the oscillation after projecting the components onto the original data (Schmeits and Dijkstra 2000), which can be used to study propagating signals. This analysis tool will be used to study the multidecadal variability and to validate POP with altimetry data.

Before applying the M-SSA analysis tool, it is necessary to pre-filter the data for each individual time series. Depending on the data set (POP, SODA or AVISO), some time series show a trend. Therefore, the trend is removed from the data. Furthermore, for each calender month the average is determined and subtracted to produce nonseasonal data and the time series is normalized. To reduce the number of spatial dimensions, a principal component analysis (PCA) is applied. A limited number of principal components (PCs) are retained which contain at least 90% of the total variance (Schmeits and Dijkstra 2000). There are some excellent studies on how to perform an M-SSA and the technical details can be found within (Vautard and Ghil 1989; Plaut and Vautard 1994; Allen and Robertson 1996; Schmeits and Dijkstra 2000; Ghil et al. 2002). All the confidence intervals, generated by red noise surrogate data while using a Monte Carlo significance test, of an M-SSA are derived from 2500 realizations (see Allen and Smith (1996)).

The spatial dimensions of the field on which the M-SSA is performed are 45° – 70°W and 3° – 20°N. The full data sets are restricted to this selection in order to partly filter out the high variable Atlantic Ocean and Amazon outflow area. This section is the downstream region of the NBC and will be used to study multidecadal variability and the

[1] https://climatedataguide.ucar.edu

[2] http://www.aviso.altimetry.fr/en/data.html

validation of POP. The NBC is represented by the region between 30° – 50°W and 3°S – 8°N, and is only studied for the multidecadal case.

b. Position of Retroflection

The observed retroflection by AVISO (see Figure 1) is persistent during boreal Autumn and Winter (Johns et al. 1990). The NBC follows the continental shelf closely and is translating northwestward where it retroflects at a certain latitude. Therefore, the coordinate system is titled by 31° clockwise to construct a convenient frame of reference to describe the NBC retroflection phenomenon. We project all the vectors onto this tilted coordinate system which results in a new zonal- (u_*) and meridional velocity (v_*). In addition, the outflow area of the Amazon is filtered out due to its high variability in time. The outflow area is based on the significant larger variance in SSH compared to the Atlantic Ocean over the full observed period. The highly variable outflow area for the modeled data is not present at a depth of 5 m and therefore not filtered out.

In order to detect the retroflection, the position (point A) is determined first along the meridional cross-section where the zonal velocity (u_*) has the largest magnitude in westward movement (see Figure 1). Secondly, at the corresponding grid cell the SSH is determined which gives an indication of the NBC (Cetina-Heredia et al. 2014). Since the retroflection is anti-cyclonic, the SSH increases towards the centre of the retroflection. Therefore, the determined SSH along the cross-section is set as a lower boundary. The upper boundary is set 16 cm higher, where SSH isolines are plotted between these boundaries (each spaced by 0.5 cm) which should result in sufficient isolines to determine the retroflection. Only representative SSH isolines are taken into account which has been accomplished by extracting the isolines which intersect the meridional cross-section twice (or more) (see Figure 1).

Each relevant SSH isoline is used until the retroflection is found, starting at the lowest SSH isoline. Each isoline is followed clockwise as in the same direction as the NBC. The position of the retroflection is determined when an isoline turns eastward. Consequently, a threshold of 31° clockwise from the geographical north (parallel to meridional cross-section) is applied to determine the turning of the current (Cetina-Heredia et al. 2014). The results were not significantly influenced by the threshold of 31° which has been investigated while slightly changing this value by ±15°. When the NBC tends to retroflect, the meridional velocity (v_*) increases significantly along the isoline. Therefore, an additional threshold for the meridional velocity near the retroflection point is applied to distinguish the current from the variable background, which is set to $v_{crit} = 20$ cm s^{-1}. Smaller values for v_{crit} allow more data points, but falsely computes the retroflection position. This might occur when the NBC is not a 'pure' zonal flow (like in Figure 1), even in the tilted coordinate system. The meridional velocity reaches the threshold easily of 20 cm s^{-1} inside the NBC, whilst the retroflection is not near the determined point.

Since the retroflection is seasonal dependent (Johns et al. 1990), the retroflection position differs in time. Besides, ring-shedding events might lead to a temporal northwestward excursion of the retroflection. These (combined) effects cause that the retroflection is not always captured by this method. In these cases, the retroflection is better determined while shifting the meridional cross-section 1° westward and performing the same analysis. If the retroflection can not be determined as well by this shifted cross-section, the cross-section (as in Figure 1) is placed 2° eastward. Only in a few cases, the retroflection is found relatively 'far' towards the east and can be detected by this cross-section. If all three cross-sections fail to capture the retroflection, it is assumed that no (or weak) retroflection is present.

The retroflection in Figure 1 is determined at 51.8°W and 8.2°N. Besides, the meridional velocity (v_*) is determined near the point of retroflection to study the current strength and whether there is a seasonal effect. Both position and velocity are determined for both data sets and are compared. Since the retroflection has the strongest magnitude during Boreal Autumn (Johns et al. 1990), it is expected that the meridional velocity shows a clear seasonal behavior near the point of retroflection.

It is possible to determine the barotropic geostrophic velocities from the SSH field for AVISO to determine the retroflection (Cetina-Heredia et al. 2014). However, the retroflection is located near the equator. While determining the geostrophic velocity from the SSH fields, grid cells around the equator within 4° deviate more than ±20 cm s^{-1} in magnitude compared to the gridded geostrophic velocity provided by AVISO. The velocities further from the equator deviate less than ±10 cm s^{-1}. Therefore, we used the gridded geostrophic velocity of AVISO to overcome the problem with large velocities near the equator.

In addition, an attempt was made to deduce the centre of the retroflection and, from this, the left limb. The centre was based by taking (tilted) zonal- and meridional cross-sections and analyzing the horizontal kinetic energy and velocity profiles. Besides, the relative vorticity was computed to determine the strongest anti-cyclonical movement to validate these findings. Unsurprisingly, this rather complicated method failed frequently. Another method which has been developed followed a similar procedure as in Dencausse et al. (2010). Although this method captures significantly accurately the retroflection, still it is not able to determine the retroflection well over the full period. In conclusion, both methods resulted in a less consistent way to determine the retroflection compared to

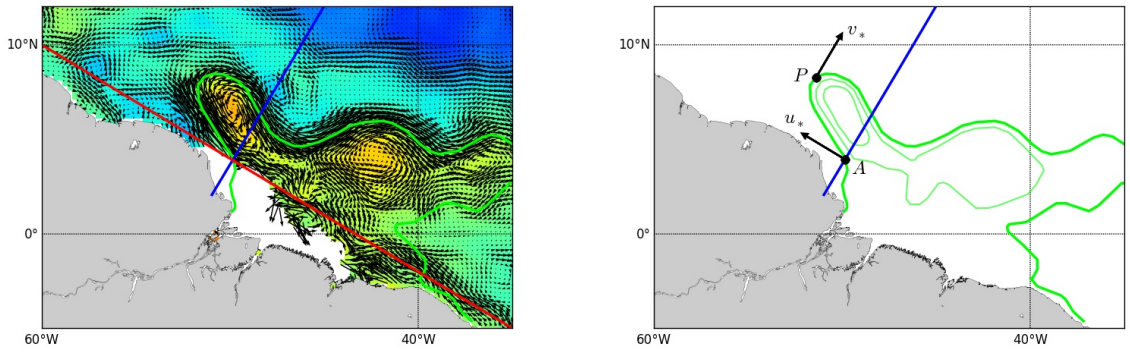

FIG. 1: Left panel: Observed geostrophic velocity (quiver) and SSH (contour) field by AVISO during October 2011. The red and blue line indicate the tilted coordinate system, rotated by 31° clockwise. The green line is an SSH isoline which represents the NBC current. Right panel: Same green SSH isoline and two additional SSH isolines. All SSH isolines intersect the blue meridional cross-section twice. The NBC is determined in point A including the zonal velocity (u_*) of maximum westward movement. The retroflection is determined at point P (51.8°W, 8.2°N) along the SSH isoline, including the meridional velocity (v_*) of the retroflection point.

the SSH isolines and geostrophic velocity method (e.g. Cetina-Heredia et al. 2014).

c. Ring-shedding

A retroflection sheds off multiple rings per year (Goni and Johns 2001). These rings have a typical diameter of 200 – 400 km and vertical structure between 500 and 1000 m (Fratantoni et al. 1995; Simmons and Nof 2002). Ring-shedding events are characterized by a southeastward retraction of the NBC (Cetina-Heredia et al. 2014). Therefore, studying the position of retroflection in time could give insights in ring-shedding frequency and whether these events are observed or modeled. However, ring-shedding events are hard to detect for monthly averages due to the temporal structure of the retroflection. Therefore, weekly averages are solely used to study ring-shedding events.

The retroflection is characterized by a longitude and latitude position. The ring-shedding events can therefore be studied in the longitude and latitude time series of the retroflection position (Dencausse et al. 2010). However, not all ring-shedding events can be detected simultaneously in both time series. Therefore, the retroflection position in time is converted to a scalar by determining the distance to an imaginary point at 60°W and 3°N. Occasionally, an NBC ring or eddy is falsely determined as the retroflection, while the actual retroflection is found more towards the southeast. These temporal mismatches (1 – 2 weeks) appear as clear spikes and will be removed by despiking the time series. The despiking procedure is shortly discussed in the appendix.

After the data preparation, for each calender month the average is determined and subtracted to produce nonseasonal data and the time series is normalized. To identify whether eddies are shed off with a certain period, a singular spectrum analysis (SSA) is applied to the time series (Ghil et al. 2002). This analysis tool is quite similar as the M-SSA, but allows only a single time series. This tool provides also dominant oscillations tested against red noise, with the same Monte Carlo significance test (Allen and Robertson 1996; Allen and Smith 1996). The technical details of the SSA tool can be found in the earlier mentioned studies. The confidence intervals of an SSA are derived from 2500 realizations (see Allen and Smith (1996)).

4. Model Validation

This section provides the results whether POP is capable of describing the NBC dynamics on short time scales compared to altimetry data provided by AVISO.

a. Position of Retroflection

The described procedure is followed for all the data sets of AVISO and POP. Firstly, all the available months of AVISO (in total 252 months) are manually checked to validate the findings and performance of the procedure. In 2% (5 months) of the observations, the retroflection is not determined accurately[3]. The majority (4 months) of these failures occur during the months February – July, when the retroflection is absent and the NBC is highly variable.

[3]Clear distinction between determined point and visible retroflection based on the geostrophic velocity field.

TABLE 1: Frequency when retroflection is absent or relative weak, based on monthly averages for AVISO and POP (available months 252 and 600, respectively).

Dataset	Total	DJF	MAM	JJA	SON
AVISO	52	7	34	11	0
POP	230	16	112	97	5

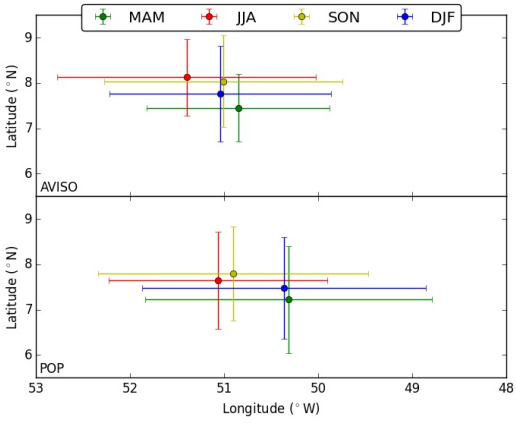

FIG. 2: Average position of the left limb of the NBC retroflection for AVISO (upper panel) and POP (bottom panel) grouped per season, the errors are 1σ.

The retroflection was absent for AVISO (POP) during 52 (230) months out of a total of 252 (600) months (see Table 1). This result shows a strong seasonal pattern in accordance with Johns et al. (1990). Especially during Spring (MAM), no or weak retroflection is present. For the remaining 200 (370) months, the positions are grouped per season (see Figure 2). There is no clear difference among the seasons. The average position from observations is 51.1°W and 7.9°N and modeled data is 50.7°W and 7.6°N.

For the remaining 200 (370) months the probability density function of the retroflection position is further analyzed as shown in Figure 3. The probability density functions cover approximately the same area and are aligned along the continental shelf. Both both profiles are inclined by 123° clockwise from the geographical north. The continental shelf was inclined by 121° (see Figure 1). However, there are differences between the data sets. The probability density function of AVISO has one grid cell with the highest frequency and some scattering near this grid cell. On the contrary, the probability density function of POP shows two grid cells of relative high frequency, leading to a more double peaked pattern. This might be related to the fact that the wind stress curl has a constant yearly cycle in POP and therefore generating more regularly NBC rings and/or eddies.

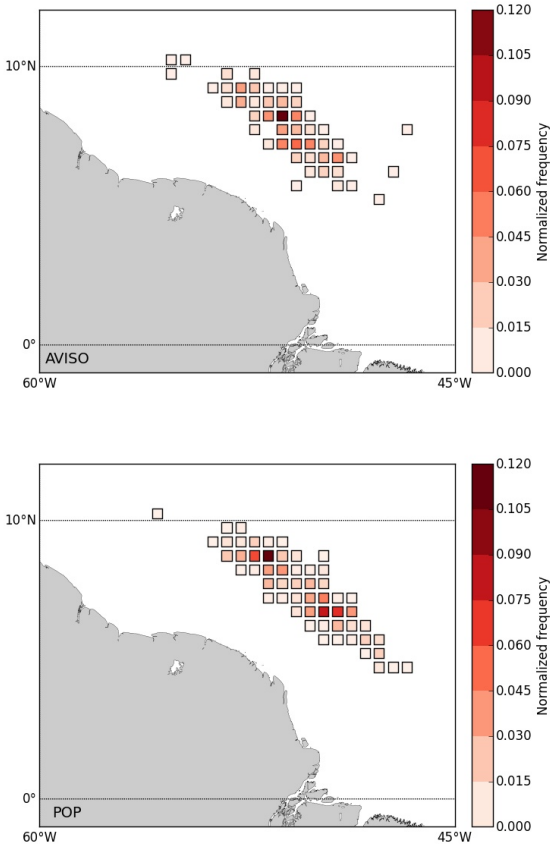

FIG. 3: Probability density of the retroflection based on monthly averages of AVISO (upper panel) and POP (lower panel) for 200 and 370 months, respectively. Note that the grid cells ($0.5° \times 0.5°$) in the figures are not the actual grids.

The meridional velocity is determined near the point of retroflection (see Figure 4). Although the position of this point is not stationary, it shows a clear seasonal pattern in accordance with Table 1. The retroflection is significantly stronger during Autumn (SON) compared to Spring (MAM). Note that the error bars are smaller during Spring due to less observations since the retroflection was frequently absent during these months.

A similar analysis has also been performed by taking weekly averages for AVISO. We analyzed 1095 weeks manually and find that in 6% (70 weeks) of the observations the retroflection is determined falsely[3] by the script. In addition, 48 weeks (69%) of these failures originate during the months February – July. Most of these failures are that an NBC ring is identified as the retroflection. Although the procedure fails more frequently for weekly averages, the average position of the retroflection is similar to monthly averages. The determined position of weekly observations is 51.0°W and 7.9°N and weekly modeled data is 50.3°W and 7.3°N.

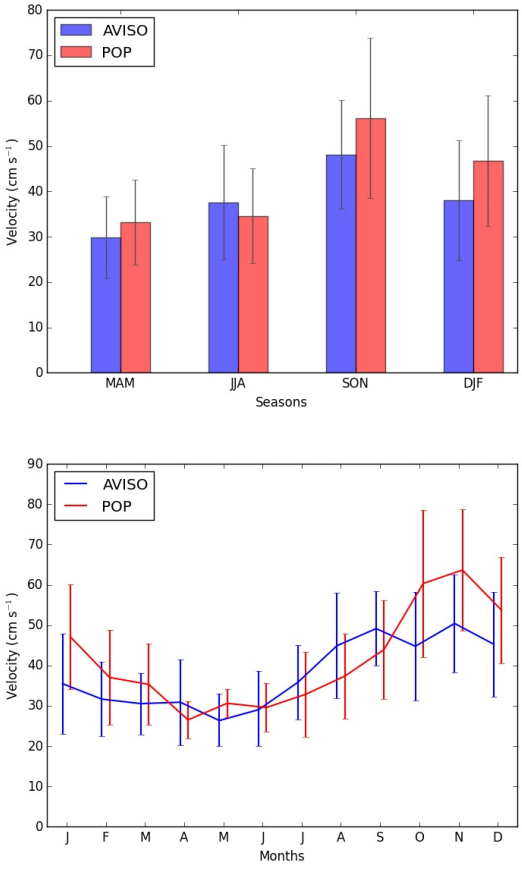

FIG. 4: Meridional velocity (v_*) determined near retroflection point (see Figure 1), grouped per seasons (upper panel) and per month (lower panel) using monthly averages of AVISO and POP. The error bars are 1σ and have a cut-off at 20 cm s^{-1}.

Although the retroflection is relatively weak or absent during March – August (see Table 1 and Figure 4), there are differences among the observations and modeled data using monthly averages. The contribution of an absent retroflection for AVISO and POP during Spring (MAM) is 65% and 49% while during Summer (JJA) is 21% and 42%, respectively. In addition, the average velocity for POP is smaller than AVISO during April – September, followed by a rapid increase after these six months. In the following six months, POP resolves the retroflection velocity on average higher than AVISO. Although the seasonality is resolved and the magnitude corresponds to the observations, the seasonality is more distinct for POP compared to AVISO. However, weekly averages show a more consistent pattern for AVISO and POP among the different seasons (see Table 2). The contributions of a weak retroflection for AVISO and POP during Spring (MAM) are 59% and 53% while during Summer (JJA) are 24% and 17%, respectively.

TABLE 2: Frequency when retroflection is absent or relative weak, based on weekly averages for AVISO and POP (available weeks 1095 and 208, respectively).

Dataset	Total	DJF	MAM	JJA	SON
AVISO	136	14	80	32	10
POP	30	7	16	5	2

b. Ring-shedding

There are 208 weekly averages available for POP, therefore we used a similar length for AVISO to compare both data sets. Johns et al. (1990) find a 40 – 60-day oscillation which is related to the intrinsic behavior of the NBC and an approximate 50-day oscillation with NBC rings and/or eddy shedding. For POP there is no significant oscillation detected over the full spectrum with such a period. However, a 50-day oscillation is observed in AVISO, but depends strongly at the start date of the time series. Although rings are shed off throughout the year, a clear southeastward retraction is not always observed. Therefore, we selected the data from March 12, 2001 – March 7, 2005 to obtain a pattern with some periodic southeastward retractions of the retroflection. The despiked time series of the position are shown in Figure 5. A southeastward retraction can be identified as a rapid decrease in distance, in the order of a few hundred kilometers.

We applied a lag-window of $M = 100$ weeks while the original data has a length of $N = 208$ weeks. The surrogate data is projected back onto the PCs of the red noise null-hypothesis basis and data basis (Schmeits and Dijkstra 2000), these results are shown in Figure 5. When a PC exceeds the 95% confidence interval in both basis, the associated frequency might be related to an oscillation which can be distinguished from red noise. The only significant oscillation has a period of 50 days, in accordance with the findings of Johns et al. (1990). Varying the lag-window length has no large influences on the period (see Table 3). However, these results are strongly dependent on the selection of the time series which also showed a 44-day oscillation during January 24, 1994 – January 19, 1998 (not shown here). Besides, for some time series the 44- or 50-day oscillation is observed either in the red noise basis or data basis, but simultaneously only during selected time windows. Therefore, these results should be interpreted with care. Note that this analysis is also performed over the full observed range (1095 weeks), but resulted in no significant oscillations.

c. Multi-channel Singular Spectrum Analysis, Temporal Variability

First, the AVISO data set is reduced to 208 weeks. The results of the M-SSA are less sensitive by varying the time span compared with the SSA. We have obtained the

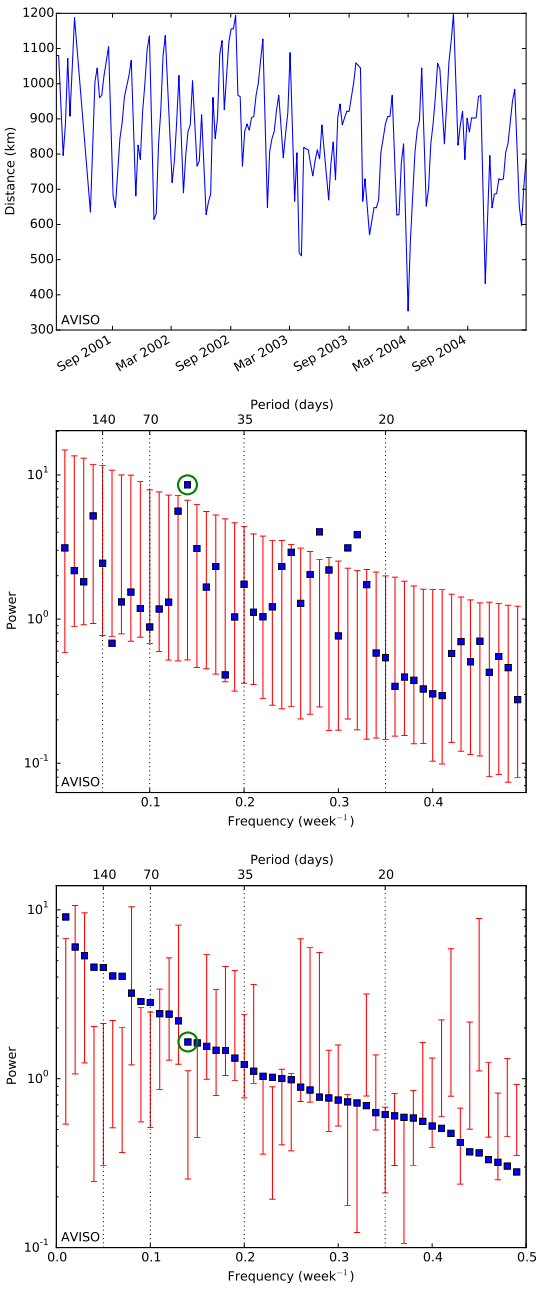

FIG. 5: Despiked retroflection position (upper panel) during March 12, 2001 – March 7, 2005. The SSA performed on the time series with the red noise basis (middle panel) and data basis (lower panel) for AVISO over a time period of 208 weeks, using a lag-window of 100 weeks. The red vertical bars are the 95% confidence intervals and the blue data points correspond to a specific PC. The circled PC appears significant for both basis with an associated period of 50 days.

TABLE 3: Significant oscillations determined from SSA of the retroflection position for both data sets where the lag-window length (M) varies between 25 – 100 weeks using a total length of $N = 208$ weeks. Note that for AVISO the periods are determined from separate sections of the full time series.

Lag-window length (weeks)	Period (days)	
	AVISO	POP
25	–	–
50	50	–
75	44, 53	–
100	44, 50	–

TABLE 4: Significant oscillations determined from M-SSA on the SSH data for both data sets where the lag-window length (M) varies between 25 – 100 weeks and total length of $N = 208$ weeks.

Lag-window length (weeks)	Period (days)	
	AVISO	POP
25	40, 52	42, 56
50	43, 51	43, 51
75	43, 52	43, 52
100	40, 55	51

weekly averages SSH from April 28, 2008 – April 16, 2012. In total, 45 and 51 PCs are retained during the pre-filtering process for AVISO and POP, respectively. We applied a varying lag-window length of $M = 25 - 100$ weeks while the original data has a length of $N = 208$ weeks for the M-SSA. The surrogate data is projected back onto the ST-PCs of the red noise null-hypothesis basis (Schmeits and Dijkstra 2000), these results are shown in Figure 6. Note that the data has also been projected on the ST-PCs data basis (not shown here) to identify whether an oscillation is significant.

Note that not all high frequencies (< 35 days) are significant since the ST-PCs data basis (not shown here) exclude some frequencies. Still, there are plenty oscillations marked as significant. These frequencies are probably not related to an intrinsic oscillation, but are likely caused by tropical instability waves (Johns et al. 1990). Therefore, all high frequency oscillations (< 35 days) are excluded from the findings (see Table 4). Note the resemblances in significant oscillations of the SSA and M-SSA in AVISO.

Both red noise spectra have three low frequency peaks below the confidence interval with an oscillation period of 180, 90 and 60 days. These peaks are the result of removing the seasonal average. Without removing the seasonal pattern, these oscillations are significant and the 43- or 51-day oscillation can not be distinguished from the surrogate

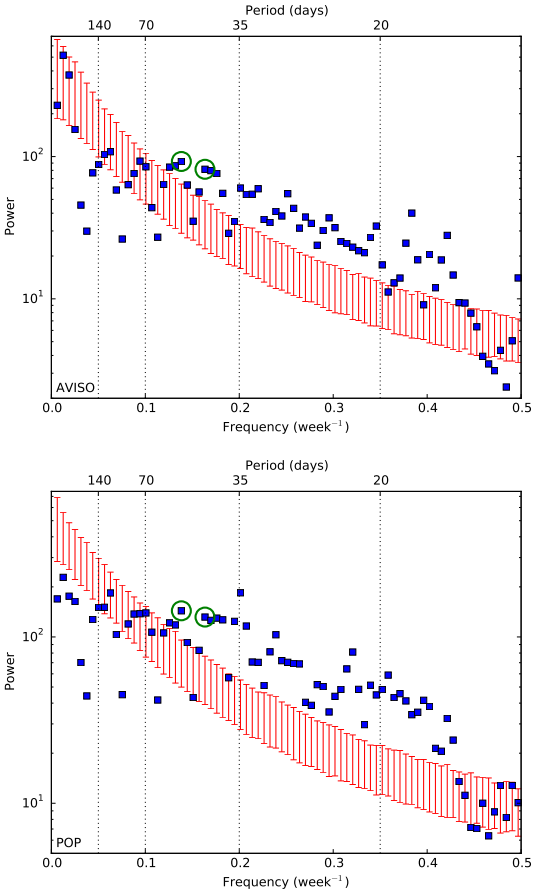

FIG. 6: The M-SSA performed on the SSH field in the red noise basis for AVISO (upper panel) and POP (lower panel) for a period of 208 weeks, using a lag-window of 50 weeks. The red vertical bars are the 95% confidence intervals and the blue data points correspond to a specific ST-PC. The circled PCs are significant in both basis (only red noise basis is shown here) with a period of 43- and 51-days (see Table 4).

noise. Besides, both data contain the same high variability for high frequencies.

Applying a lag window of 50 weeks, the Monte Carlo significance test provides two potential oscillations with two different periods. The relevant ST-PCs were determined by the same criteria as in Plaut and Vautard (1994): the lag-correlation remains close to a sine function and the two successive extrema, on each side of 0, are larger than 0.5 in absolute magnitude. It is possible that there are more pairs with the same oscillation, however the highest order ST-PC is selected to isolate the oscillation. Such a pair is shown in Figure 7a.

Using the appropriate ST-PC pairs, one can reconstruct the RCs (Ghil et al. 2002). For AVISO, RC pairs 34 – 35 and 23 – 24 are related to the 43-day and 51-day oscillation, respectively. We expect to observe a propagating signal along the continental shelf associated with ring-shedding events for RC pair 23 – 24 (Johns et al. 1990). Therefore, we placed a window near the continental shelf and determined the SSH anomaly in time (see Figure 7b). The Hovmoller diagram shows a clear propagating signal in time with a speed of 14 km day^{-1} between 48° – 57°W. In addition, there is a signal propagating eastward between 45° – 48°W. This might be related to the re-absorption of NBC rings and eddies or simply the NBC retroflection. However, the 43-day oscillation shows in some extend a similar pattern (not shown here). Yet, this signal is only visible from November 2010 – April 2012 and propagates with a slightly higher velocity of 19 km day^{-1}.

TABLE 5: Significant oscillations determined from M-SSA on the SSH data for AVISO over the full observed period where the lag-window length (M) varies between 25 – 100 weeks.

Lag-window length (weeks)	Period (days)
25	–
50	48, 55, 63
75	40, 48, 63
100	43, 48, 53

For POP, RC pairs 23 – 24 and 30 – 31 are related to the 43-day and 51-day oscillation, respectively. Neither RC pairs 23 – 24 nor 30 – 31 showed a proper translating signal along the continental shelf as in Figure 7b. Using other lag windows for POP did not result in any improvements. Remarkably, for some lag windows the signal propagates towards the retroflection. This is very unlikely since the NBC is propagating in the first 700 m towards the Lesser Antilles and therefore eddies nor NBC rings should propagate upstream.

We also investigated the full time series of AVISO. We processed the data in a similar way and retrieved 97 PCs in the pre-filtering process. The lag-window length is varying between 25 – 100 weeks where the original data contains 1095 weeks. There are multiple oscillations detected which are listed in Table 5. The same propagating signals are observed as in Figure 7b while using the RCs which are associated with the 50-day oscillation.

5. Results and Analysis

The results of the multidecadal variability in the NBC are presented in this section. Furthermore, the results of a teleconnection with the Southern Ocean and some additional multidecadal variability in the NBC transport are presented.

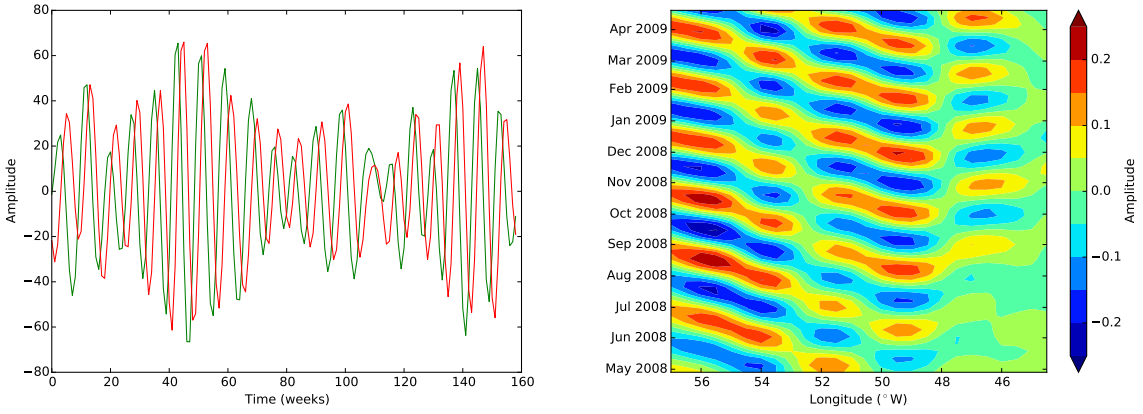

(a) ST-PC pair 23 – 24

(b) Hovmoller diagram of RC pair 23 – 24

FIG. 7: Left panel: Time series of ST-PC pair 23 – 24, associated with a 51-day oscillation determined from the AVISO output. Right panel: Hovmoller diagram using RC pair 23 – 24 from April 28, 2008 – April 16, 2012. The SSH anomalies are shown along 8° – 10°N as a function of longitude and time.

a. Multidecadal Variability

The current time series of AVISO is insufficient to study multidecadal variability. Therefore, all the monthly average fields of POP are used to study multidecadal variability in SSH. Since we are interested in variability on long time scales, it is possible to reduce both spatial as temporal resolution without losing too much information. The grid size of the field is adapted to 0.8° × 0.8° by averaging over four individual grid cells. Furthermore, the time resolution is reduced by averaging over two months. The data for each individual grid cell is in a similar way processed as AVISO: detrended, nonseasonal and normalized. During the pre-filtering process, 74 PCs are retained. The lag-window varies between 650 – 800 months (Table 6). Note that during the M-SSA the actual lag window is set at exactly half, since the time resolution is bimonthly. The results of the data and red noise basis, while using a lag-window of 680 months, are shown in Figure 8.

The data set of SODA is analyzed in a similar way. However, the spatial and temporal resolution have not been reduced as in POP. During the pre-filtering process, 53 PCs are retained to reduce dimensions. A varying lag-window did not result in any significant oscillations at the 95% confidence level. Remarkable, there were two significant oscillations detected at the 90% confidence interval (Table 6).

The outflow area of the NBC is highly variable. This can also be observed by applying the M-SSA on the NBC (30° – 50°W and 3°S – 8°N). First of all, the amount of retained PCs in the pre-filtering processes are reduced to 14 and 15 for POP and SODA, respectively. Secondly, the results of the M-SSA of SODA appear to be significant at the 95% confidence level and have an additional oscillation of 28 years (see Table 7). There are no additional oscillations found in POP.

TABLE 6: Significant oscillations determined from M-SSA on the SSH data for POP and SODA over the full observed period where the lag-window length (M) varies between 650 – 800 months, near the NBC outflow area.

Lag-window length (months)	Period (years)	
	POP	SODA
650	–	29[4], 43[4]
680	48	42[4]
710	47	–
800	45	–

TABLE 7: Significant oscillations determined from M-SSA on the SSH data for POP and SODA over the full observed period where the lag-window length (M) varies between 650 – 800 months, near the NBC

Lag-window length (months)	Period (years)	
	POP	SODA
650	–	29, 43
680	48	28, 42
710	47	–
800	45	–

To rule out the effect of the wind-stress forcing on the SSH, the wind-stress curl is determined over the field of interest. The wind-stress curl in POP showed a repeating yearly cycle without any forcing. The wind-stress curl of SODA is not constant in time. Yet, it did not contain a multidecadal variability and is deduced as a white signal.

[4]Period significant at the 90% confidence level

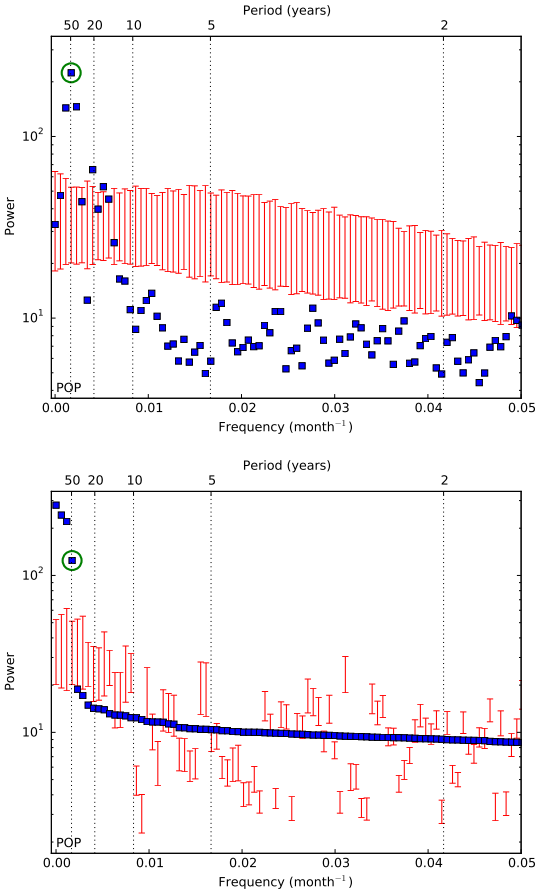

FIG. 8: The M-SSA performed on the SSH field in the red noise basis (upper panel) and data basis (lower panel) for POP for a period of 2415 months, using a lag-window of 680 months. The red vertical bars are the 95% confidence intervals and the blue data points correspond to a specific ST-PC. The circled PCs are significant in both basis with a period of 48 years (see Table 6).

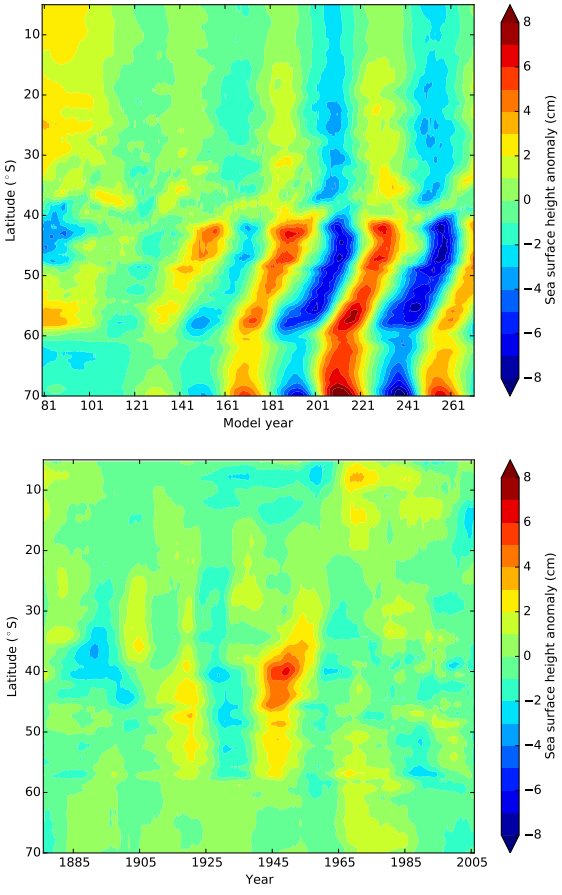

FIG. 9: Hovmoller diagrams of SSH anomalies near the Southern Ocean in POP (upper panel) and SODA (lower panel). The SSH anomalies are shown along 5° – 55°W. The data is smoothed while applying a running mean of ten years. Note that the figures have a different time axis.

The period is slightly decreasing while increasing the lag-window, as shown in Table 6 and 7. This is related to the length of the lagged time series, which decreases for larger lag-windows and results in a larger spacing between two frequencies (Allen and Smith 1996).

b. Teleconnection Southern Ocean

We placed a rectangular section in the Atlantic Ocean to deduce whether there is any propagating signal originating from the Southern Ocean. First, the SSH is determined along 5° – 55°W over all available months in POP and SODA. The data of SODA is detrended for each individual grid cell. At each latitude, the average SSH is determined and subtracted to retain SSH anomalies. Subsequently, these time series are smoothed by applying a running mean of ten years. This result is shown in Figure 9 between 5° – 70°S.

In POP there is a clear northward propagating SSH anomaly in the Southern Ocean (40° – 60°S) with a speed of 78 km year^{-1}. This speed is typically associated with Rossby waves (Chelton and Schlax 1996). The northward propagating signal disappears at 40°S. The propagating signal is oscillating and has an approximate period of 45 years. Furthermore, between 5° – 40°S the same oscillation of 45 years as in the Southern Ocean is present, but the pattern is stationary. Besides, the SSH anomalies are less in magnitude compared to the Southern Ocean. These results suggest that the anomalies from the Southern Ocean submerge near 40°S and are almost instantly distributed by the Southern Atlantic Subtropical Gyre.

To investigate whether the multidecadal signal submerges, the same analysis as the SSH anomaly is performed over each individual depth layer for both temperature, salinity and ocean heat content (OHC). The tem-

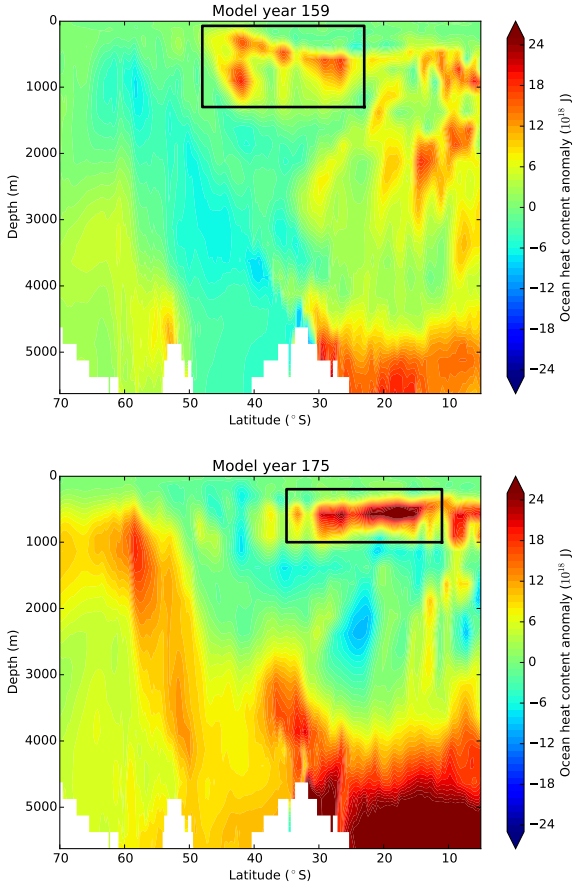

FIG. 10: Positive anomaly in the ocean heat content (OHC) in the marked region of the POP output. The anomalies are determined along 5° – 55°W for each individual depth layer. The positive anomaly submerges near 40°S (upper panel, model year 159) and propagates towards the north (lower panel, model year 175). The marked regions in both figures are linked to each other.

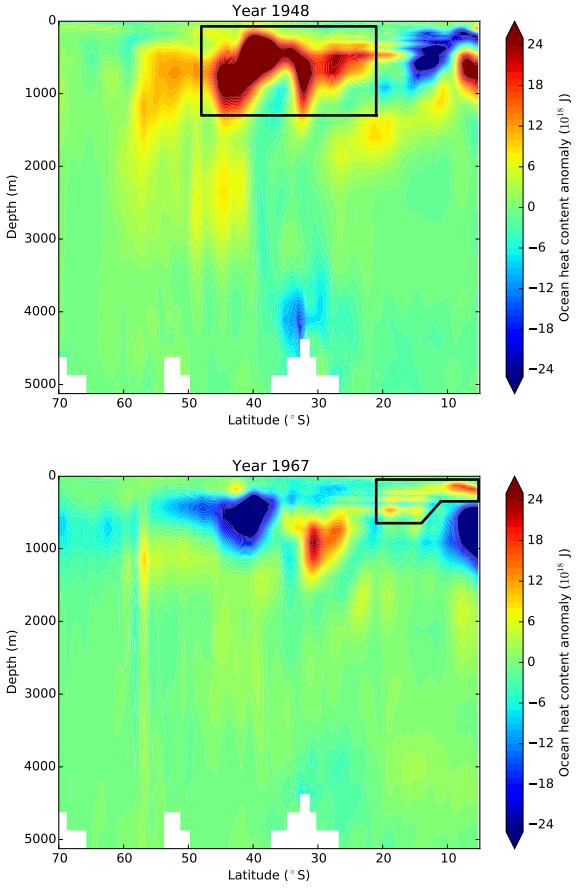

FIG. 11: Positive anomaly in the ocean heat content (OHC) in the marked region of the SODA output, similar as in Figure 10. The positive anomaly submerges near 40°S (upper panel, year 1948) and propagates towards the north (right panel, model year 1967) where it re-emerges near the surface. The marked regions in both figures are linked to each other.

perature, salinity and pressure dependency of water were taken into account while computing the OHC anomalies (Millero and Chen 1980). Studying these anomalies in time revealed that the northward propagating signal submerges at 40°S, reaching depths up to 1 km and extends till 5°S. An example of this process for a positive OHC anomaly is shown in Figure 10. The positive anomaly originating from the Southern Ocean submerges near 40°S in model year 159 and propagates northwards between model year 159 – 175 (not shown here). In model year 175, the anomaly reaches 10°S. At this latitude, the anomalies can be transported by the South Equatorial Current (SEC), where the formation of the NBC starts (Johns et al. 1998). The NBC will cross the equator and streams towards the NBC region.

There is not a propagating signal observed in the Southern Ocean for SODA. During the period 1915 – 1980, there might be a weak oscillation of 28 years and this signal is stationary. This period is found to be significant in the NBC (see Table 7). In 1945 near 40°S, a positive SSH anomaly seems to propagate northwards with a speed of 108 km year^{-1}. However, this is the only propagating signal near the Southern Ocean.

The temperature, salinity and OHC anomalies revealed that some anomalies submerge near 40°S and extend northwards. However, the majority of these anomalies are less in magnitude compared to POP and did not propagate northwards. In 1940, a relative strong positive OHC anomaly submerges at 40°S and propagates towards the north where it re-emerges to the surface at 10°S in 1967, as shown in Figure 11. This is in line with the observed posi-

tive SSH anomaly as in Figure 9 during the period of 1940 – 1970. Therefore, linking the positive SSH anomaly at 40°S and 10°S, we find a mean velocity of 170 km year^{-1}. Note that this is the only signal observed which is able to reach 10°S.

The reason of the submerging signal can be explained by two effects. Firstly, there is a weak annual mean Ekman downwelling of 0 – 5 cm day^{-1} near 40°S (Xie and Hsieh 1995). Secondly, the water near the surface in the Southern Atlantic Subtropical Gyre is overall highly saline (35 – 37 g kg^{-1}) and warmer (15 – 25°C) than its surroundings, for example the fresh (33 – 35 g kg^{-1}) and cold water (0 – 5°C) from the Southern Ocean. The thermal expansion overcomes the saline contraction, leading to a water mass with a slightly lower density in the Subtropical Gyre compared to water from the Southern Ocean (see Figure 12). The isopycnals show a clear meridional gradient between 30 – 60°S in the POP output, even at 1 km below the surface. This pattern is disturbed in SODA, but shows also a lower density in the subtropical gyre. The boundary between these water masses is located near 40°S. The combination of Ekman downwelling and stratification cause the signal to submerge. Due to the strong equatorial Ekman upwelling (40 cm day^{-1}) (Xie and Hsieh 1995), the anomalies can surface.

c. Transport and Sea Surface Height

Since POP and SODA resolve the velocity at multiple depth levels, the opportunity arises to determine the transport in time. Since the SOM influences the OHC (Le Bars et al. 2016), the slope in isopycnals might change, leading to a stronger or weaker baroclinic instability which results in more or less transport. Therefore, there might be a multidecadal signal in the transported water by the NBC. Three cross-sections were placed at 40°W, 50°W and 60°W along 5°S – 10°N, 1°S – 12°N, 7°N – 18°N, respectively. The zonal velocity is mainly directed towards the west in the first 700 m, whereas at greater depths the Atlantic North Equatorial Undercurrent moves eastwards. The average velocity is determined along a cross-section at each depth level up to 700 m. This depth profile is linearly integrated to determine the (westward) transport. This has been accomplished for all available months for POP and SODA.

In addition, we determined the average SSH over 7°S – 20°N and 38° – 62°W. The time series for SSH and transport sections show in some extend a trend and seasonal pattern. Therefore, all the time series are detrended, the seasonal signal is removed and are normalized. The time series are smoothed by applying a running mean of several months. An example of the time series of the SSH and transport sections are shown in Figure 13, while applying a running mean of 150 months. Note the periodic

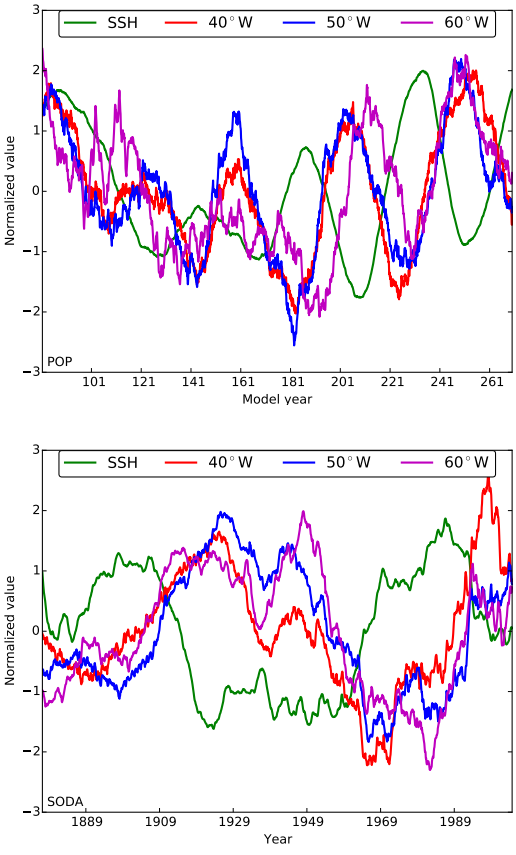

FIG. 13: Time series of average SSH field and westward transport at three cross-sections for POP (upper panel) and SODA (lower panel). All time series are detrended, non-seasonal, normalized and smoothed by applying a running mean of 150 months.

signal in SSH in POP. The period in SSH is approximately 44 years, which is in line with the M-SSA results.

The time series of the transport sections have a phase difference with the SSH. In POP it is not clear whether the SSH lags or leads the transport sections. In SODA, the SSH leads the transport sections. The results while lagging the transport sections to the SSH are displayed in Table 8. Changing the length of the running mean has no large influences on the lag between SSH and transport sections. When the transport sections are leading, the maximum correlations were slightly lower in POP. Besides the corresponding lag changed, for example from 200 months to -300 months. This demonstrates that the transport in POP is also periodic with an approximate period of 500 months (42 years). The transport section for SODA showed no signs of periodicity while leading the transport sections to SSH.

The westward transport determined at 40°W is lagging the SSH of approximate 17 years (210 months) and 22 years (267 months) for POP and SODA, respectively.

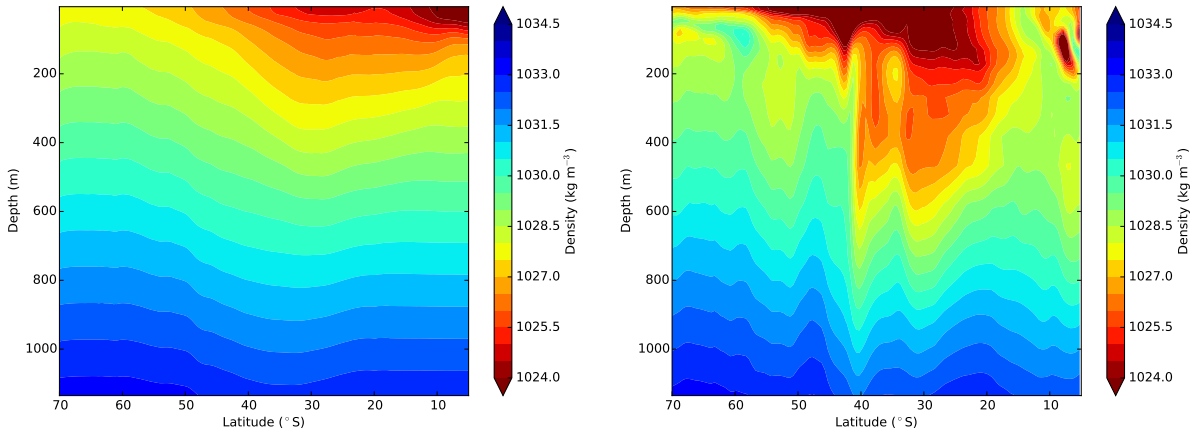

(a) Average density, POP

(b) Average density, SODA

FIG. 12: The average density profiles along 5° – 55°W for the POP (left panel) and SODA (right panel) output, for the first 1000 m. The temperature, saline and pressure dependency of water were taken into account while determining the density (Millero and Chen 1980).

TABLE 8: Three sections over which the westward transport is determined and compared to the field average SSH for POP and SODA. All time series are smoothed by taking moving averages. The transport sections are lagged to the SSH up to 500 months, where the maximum correlation (r) and corresponding lag (τ) are determined over this interval. The errors on the correlation coefficient are the 95% confidence interval.

Model	Moving average (months)	Transport sections 40°W		50°W		60°W	
		r	τ (months)	r	τ (months)	r	τ (months)
POP	90	0.72 ± 0.02	208	0.61 ± 0.03	197	0.62 ± 0.03	250
SODA		0.67 ± 0.03	251	0.66 ± 0.03	423	0.66 ± 0.03	458
POP	120	0.73 ± 0.02	209	0.63 ± 0.03	200	0.67 ± 0.02	253
SODA		0.75 ± 0.02	255	$0.74^{+0.02}_{-0.03}$	396	0.69 ± 0.03	465
POP	150	0.74 ± 0.02	213	0.63 ± 0.03	204	0.69 ± 0.02	247
SODA		0.81 ± 0.02	264	0.81 ± 0.02	390	0.73 ± 0.03	489
POP	180	0.74 ± 0.02	213	0.64 ± 0.03	216	0.69 ± 0.02	221
SODA		$0.85^{+0.01}_{-0.02}$	268	$0.86^{+0.01}_{-0.02}$	402	$0.76^{+0.02}_{-0.03}$	464
POP	300	0.76 ± 0.02	209	0.64 ± 0.03	216	0.69 ± 0.02	221
SODA		0.92 ± 0.01	295	0.95 ± 0.01	414	0.92 ± 0.01	467

This is the only cross-section which show in some extend a similar lag between the two models. The remaining cross-sections show no similarities in maximum lag. This is probably related due to the fact that SODA is well capable of resolving the NBC and North Equatorial Counter Current (NECC), which are located near 40°W. This has been tested while comparing the SSH of each individual grid cell in AVISO and SODA during 1993 – 2010. Note that the grid of AVISO is mapped onto the grid of SODA. The correlation between SODA and AVISO near the NBC and NECC was high (0.75 – 0.95). However the retroflection and downstream region was poorly resolved by SODA compared to AVISO, where cross-section 50°W and 60°W are situated. Besides, POP is in an equilibrium state and therefore shows a periodic pattern in SSH and transport sections.

6. Discussion and Conclusion

The M-SSA analysis on the POP output shows a significant oscillation with a corresponding period of 45 – 50 years in the NBC and outflow area. This period is related to the SOM (Le Bars et al. 2016), leading to a teleconnection between the SOM and the NBC. There is some clear evidence that the multidecadal signal has a Southern Ocean origin. First of all, the SSH anomalies show that the signal is propagating northwards with a speed of 78 km year^{-1}. Secondly, the signal submerges at 40°S due to density differences, but can still be traced below the surface while studying temperature and OHC anomalies. The surface water of the Southern Atlantic Ocean are mainly transported north by the AMOC (Rahmstorf 2002; Kuhlbrodt et al. 2007). The multidecadal signal is able to

reach 10°S where the formation of the NBC starts (Johns et al. 1998). The SEC flows towards the NBC region where the multidecadal variability is observed in SSH. The same multidecadal variability has also been found in three transport sections near the NBC while lagging the transport sections to the SSH. This variability in transport can be explained to changes in baroclinic instability due to a significant change in OHC of the SOM (Le Bars et al. 2016).

The M-SSA analysis on the SODA output showed some different results. Two oscillations with a period of 28 and 42 years are found in the NBC. The outflow area of the NBC is too variable to find significant oscillations. Besides, the time series is relative 'short' compared to POP. There might be a weak oscillation in SSH of 28 years in the Southern Ocean, but only visible during 1915 – 1980. There were no signs of the 42-year oscillations. A positive OHC anomaly is propagating northwards during 1940 – 1970 at similar depths as POP. This anomaly reaches eventually 10°S where it re-emerges to the surface. There was no sign of multidecadal variability in the transports section. Still, the transport in the NBC lags the SSH. The SODA output reveals that anomalies from the Southern are able to propagate northwards, similar as in POP. However, it is not observed very often in SODA.

The M-SSA allows the usage of colored noise (Allen and Robertson 1996; Allen and Smith 1996). During this study, the variability in SSH was tested against red noise. However, the color spectrum of SSH variability is not completely red (Hughes and Williams 2010), questioning the outcomes of the M-SSA. Though, the average SSH in POP (as in Figure 13) shows a clear oscillation pattern with a period of approximate 44 years. The M-SSA on the SSH variability can be improved, but already shows the expected variability in SSH.

The intrinsic behavior of the NBC is correctly resolved in POP compared to altimetry data. The probability density profiles of the NBC retroflection are inclined along the continental shelf but POP shows a double peaked pattern, probably related to the periodic wind forcing. The velocity of retroflection is in the same order, but POP has a more distinct seasonal pattern. The stronger seasonality behavior is also observed in the absence of the retroflection, which is more often in POP (38%) than AVISO (21%). Besides, ring-shedding events and eddies are modeled but appear more regularly in POP.

Both model and observations show the same period of 43 and 51 days. The 51-day oscillation is related to ring-shedding (Johns et al. 1990), also demonstrated by the SSA analysis of the retroflection position in time. The high frequencies (20 – 30 days) observed in both data sets are related to tropical instability waves (Johns et al. 1990). The 43- and 51-day oscillation in AVISO (see Figure 7b) are propagating by 19 km day^{-1} and 14 km day^{-1}, respectively. These velocities are similar with the findings of Goni and Johns (2001) and Fratantoni and Glickson (2002) and the physical meaning of these RCs are NBC rings and/or eddies. There were no propagating signals observed towards the Lesser Antilles in POP.

The multidecadal variability, with a period of 45 – 50 years, in the NBC has a Southern Ocean Origin (Le Bars et al. 2016), connecting the SOM to the NBC. This teleconnection has been investigated by studying SSH, temperature, salinity and OHC anomalies in the Southern Atlantic Ocean. These anomalies are observed near the surface and propagate northwards by the influence of the AMOC (Rahmstorf 2002; Kuhlbrodt et al. 2007). The multidecadal variability is also observed in the NBC transport, due to changes in baroclinic instabilities which is related to the significant OHC variations of the SOM (Le Bars et al. 2016). The data assimilation provided by SODA showed no clear multidecadal variability, but is able to demonstrate that anomalies can propagate northwards from the Southern Ocean. Further teleconnections, for example the AMOC, need to be analyzed to investigate the full influence of the SOM on the ocean, which will eventually also affects the atmosphere (Le Bars et al. 2016). Furthermore, a slowing down of the AMOC (Bryden et al. 2005) needs to be studied and the effects on the NBC and the multidecadal variability. This is a more likely scenario than the control run of POP. Still, longer observations records are crucial to study multidecadal variability, which will lead to a better understanding of the intrinsic behavior of the ocean and help to improve models such as POP.

Acknowledgments. The first author would like to sincerely thank all the co-authors for their support and countless suggestions during this master thesis at the Utrecht University. The IMAU is thanked for using their facilities during this project. Aleid, Brenda, Robby and Tjebbe are thanked for their support and advice. We would like to thank Michael Klip-huis (IMAU–UU) for his kind assistance and providing the data of the POP model.

APPENDIX

Despiking procedure

The despiked procedure applies two criteria to identify a spike. Suppose a time series of length N:

$$T_i = (x_1,\, x_2,\, \ldots\, ,\, x_N) \tag{A1}$$

where i is the time index. Sometimes the retroflection is absent or weak, therefore all the missing data are interpolated between two observations to obtain a continuous time series. A sliding window of 3 unit time scans the full time series, where observation x_i is subtracted from the average of the adjacent data points x_{i-1} and x_{i+1}. This is called the 'difference' and indicates how much a point

is situated from the neighbouring observations. The difference of x_1 (x_N) uses the average of x_2 and x_3 (x_{N-2} and x_{N-1}). The next procedure is determining the average, or so-called 'box', with the same sliding window over the 'difference' including the same procedure for the end points. This is followed by taking multiple, but separate sections (i.e. 10 unit time long segments) of the 'difference' and combining these sections, where the average (μ_{ref}) and standard deviation (σ_{ref}) are determined over the combined sections. This gives a reference for the full 'difference'. Points which lie further than $3\sigma_{ref}$ from μ_{ref} are probably spikes and must not be integrated into the reference section. Therefore, other sections are chosen to work around these spikes.

Using the appropriate μ_{ref} and σ_{ref}, one can determine how much a point's 'difference' is separated from μ_{ref}, expressed in σ_{ref}. If a point is separated further than $n\ \sigma_{ref}$, where n is a value of choice (i.e. > 2.8), this point is marked as a potential spike. However, bright sources (such as the southeastward retraction) will be identified as a spike. Therefore, the second criteria is that if a point's 'difference' increases faster than it's 'box' value, the point is marked as a spike. Spikes are removed by interpolating between two 'healthy' points. This procedure can be applied by reading in the data both ways and slightly lowering n, multiple times. The threshold for n should be based on the amount of removed spikes. If this amount stays constant for subsequent n's, the data is probably despiked sufficiently. This method is also described by SURF – SCUBA User Reduction Facility[5].

References

Allen, M. R., and A. W. Robertson, 1996: Distinguishing modulated oscillations from coloured noise in multivariate datasets. *Climate Dynamics*, **12 (11)**, 775–784, doi:10.1007/s003820050142.

Allen, M. R., and L. A. Smith, 1996: Monte Carlo SSA: Detecting Irregular Oscillations in the Presence of Colored Noise. 3373–3404 pp.

Bryden, H. L., H. R. Longworth, and S. A. Cunningham, 2005: Slowing of the Atlantic meridional overturning circulation at 25 N. *Nature*, **438 (7068)**, 655–657.

Carton, J. A., and B. S. Giese, 2008: A reanalysis of ocean climate using simple ocean data assimilation (soda). *Monthly Weather Review*, **136 (8)**, 2999–3017.

Cetina-Heredia, P., M. Roughan, E. V. Sebille, and M. a. Coleman, 2014: Long-term trends in the East Australian Current separation latitude and eddy driven transport. *Journal of Geophysical Research: Oceans*, **119 (7)**, 4351–4366, doi:10.1002/2014JC010071.Received.

Chelton, D. B., and M. G. Schlax, 1996: Global observations of oceanic rossby waves. *Science*, **272 (5259)**, 234.

Cheng, L., and J. Zhu, 2014: Artifacts in variations of ocean heat content induced by the observation system changes. *Geophysical Research Letters*, **41 (20)**, 7276–7283.

[5] http://www.strw.leidenuniv.nl/docs/starlink/sun216.htx/node66.html

Condie, S. A., 1991: Seperation and recirculation of the North Brazil Current. *Journal of Marine Research*, **49 (December)**, 1–19.

Csanady, G. T., 1985: A zero potential vorticity model of the North Brazilian Coastal Current. *Journal of Marine Research*, **43 (3)**, 553–579, doi:10.1357/002224085788440321.

Dencausse, G., M. Arhan, and S. Speich, 2010: Spatio-temporal characteristics of the Agulhas Current retroflection. *Deep Sea Research Part I: Oceanographic Research Papers*, **57 (11)**, 1392–1405, doi:10.1016/j.dsr.2010.07.004, URL http://linkinghub.elsevier.com/retrieve/pii/S0967063710001561.

Fratantoni, D. M., and D. a. Glickson, 2002: North Brazil Current Ring Generation and Evolution Observed with SeaWiFS*. *Journal of Physical Oceanography*, **32 (3)**, 1058–1074, doi:10.1175/1520-0485(2002)032⟨1058:NBCRGA⟩2.0.CO;2.

Fratantoni, D. M., W. E. Johns, and T. L. Townsend, 1995: Rings of the North Brazil Current: Their structure and behavior inferred from observations and a numerical simulation. *Journal of Geophysical Research*, **100 (C6)**, 10 633, doi:10.1029/95JC00925.

Ghil, M., and Coauthors, 2002: Advanced spectral methods for climate time series. *Reviews of Geophysics*, **40 (1)**, 3.1–3.41, doi:10.1029/2001RG000092.

Goni, G. J., and W. E. Johns, 2001: A census of North Brazil current rings observed from TOPEX/POSEIDON altimetry: 1992-1998. *Geophysical Research Letters*, **28 (1)**, 1–4, doi:10.1029/2000GL011717.

Hallberg, R., 2013: Using a resolution function to regulate parameterizations of oceanic mesoscale eddy effects. *Ocean Modelling*, **72**, 92–103, doi:10.1016/j.ocemod.2013.08.007, URL http://dx.doi.org/10.1016/j.ocemod.2013.08.007.

Hughes, C. W., and S. D. Williams, 2010: The color of sea level: Importance of spatial variations in spectral shape for assessing the significance of trends. *Journal of Geophysical Research: Oceans*, **115 (C10)**.

Johns, W. E., T. N. Lee, R. C. Beardsley, J. Candela, R. Limeburner, and B. Castro, 1998: Annual Cycle and Variability of the North Brazil Current. *Journal of Physical Oceanography*, **28 (1)**, 1–26, doi:10.1175/1520-0485(1998)028⟨0103:ACAVOT⟩2.0.CO;2.

Johns, W. E., T. N. Lee, F. A. Schott, R. J. Zantopp, and R. H. Evans, 1990: The North Brazil Current Retroflection: Seasonal Structure and Eddy Variability. *Journal of Geophysical Research*, **95**, 103–120.

Kuhlbrodt, T., A. Griesel, M. Montoya, A. Levermann, M. Hofmann, and S. Rahmstorf, 2007: On the driving processes of the Atlantic meridional overturning circulation. *Reviews of Geophysics*, **45 (2)**.

Le Bars, D., H. A. Dijkstra, and J. P. Viebahn, 2016: A Southern Ocean Mode of Multidecadal Variability. *Geophysical Research Letters*, **43 (5)**, 2102–2110.

Le Bars, D., J. V. Durgadoo, H. a. Dijkstra, a. Biastoch, and W. P. M. De Ruijter, 2014: An observed 20-year time series of Agulhas leakage. *Ocean Science*, **10 (4)**, 601–609, doi:10.5194/os-10-601-2014.

Millero, F., and C. Chen, 1980: A new high pressure equation of state for seawater. Elsevier, URL http://www.sciencedirect.com/science/article/pii/0198014980900163, 255–264 pp.

Plaut, G., and R. Vautard, 1994: Spells of Low-Frequency Oscillations and Weather Regimes in the Northern Hemisphere. 210–236 pp., doi: 10.1175/1520-0469(1994)051⟨0210:SOLFOA⟩2.0.CO;2.

Rahmstorf, S., 2002: Ocean circulation and climate during the past 120,000 years. *Nature*, **419 (6903)**, 207–214.

Rühs, S., K. Getzlaff, J. V. Durgadoo, A. Biastoch, and C. W. Böning, 2015: On the suitability of North Brazil Current transport estimates for monitoring basin-scale AMOC changes. *Geophysical Research Letters*, n/a–n/a, doi:10.1002/2015GL065695, URL http://doi.wiley.com/10.1002/2015GL065695.

Schmeits, M. J., and H. A. Dijkstra, 2000: Physics of the 9-Month Variability in the Gulf Stream Region : Combining Data and Dynamical Systems Analyses. *Journal of Physical Oceanography*, **30 (1995)**, 1967–1987, doi:10.1175/1520-0485(2000)030⟨1967:POTMVI⟩2.0.CO;2.

Simmons, H. L., and D. Nof, 2002: The Squeezing of Eddies through Gaps. *Journal of Physical Oceanography*, **32 (1)**, 314–335, doi:10.1175/1520-0485(2002)032⟨0314:TSOETG⟩2.0.CO;2.

Smith, R., and Coauthors, 2010: The Parallel Ocean Program (POP) reference manual: Ocean component of the Community Climate System Model (CCSM). *Rep. LAUR-01853*, **141**, 1–141, URL http://nldr.library.ucar.edu/repository/collections/OSGC-000-000-000-954.

Vautard, R., and M. Ghil, 1989: Singular Spectrum Analysis in Nonlinear Dynamics, with Applications, to Paleoclimatic Time Series. *Physica D*, **35**, 395–424.

Xie, L., and W. W. Hsieh, 1995: The global distribution of wind-induced upwelling. *Fisheries Oceanography*, **4 (1)**, 52–67.